

# Distilling foundation models for robust and efficient models in digital pathology

Alexandre Filioit<sup>1,†,\*</sup>, Nicolas Dop<sup>\*</sup>, Oussama Tchita<sup>1</sup>, Auriane Riou<sup>1</sup>, Thomas Peeters<sup>2</sup>, Daria Valter<sup>2</sup>, Marin Scalbert<sup>2</sup>, Charlie Saillard<sup>2</sup>, Geneviève Robin<sup>1</sup>, Antoine Olivier<sup>1,†</sup>.

<sup>1</sup> Owkin, Inc, <sup>2</sup> Biotimus, Inc.

† Corresponding authors.

\* Equal contribution.

{alexandre.filioit, oussama.tchita, auriane.riou, genevieve.robin, antoine.olivier}@owkin.com, {thomas.peeters, daria.valter, marin.scalbert, charlie.saillard}@biotimus.com, nicolas.dop@student-cs.fr

**Abstract.** In recent years, the advent of foundation models (FM) for digital pathology has relied heavily on scaling the pre-training datasets and the model size, yielding large and powerful models. While it resulted in improving the performance on diverse downstream tasks, it also introduced increased computational cost and inference time. In this work, we explore the distillation of a large foundation model into a smaller one, reducing the number of parameters by several orders of magnitude. Leveraging distillation techniques, our distilled model, H0-mini, achieves nearly comparable performance to large FMs at a significantly reduced inference cost. It is evaluated on several public benchmarks, achieving 3rd place on the HEST benchmark and 5th place on the EVA benchmark. Additionally, a robustness analysis conducted on the PLISM dataset demonstrates that our distilled model reaches excellent robustness to variations in staining and scanning conditions, significantly outperforming other state-of-the-art models. This opens new perspectives to design lightweight and robust models for digital pathology, without compromising on performance.

**Keywords:** Digital pathology · Self-supervised learning · Distillation · Foundation models.

## 1 Introduction

In recent years, representation learning models have revolutionized computational pathology (CPATH) by providing efficient models that can serve for a variety of tasks, involving biomarker prediction [20,28,33], gene expression prediction [12,13,19,30], whole slide image (WSI) and tissue classification [31,39] or survival analysis [6]. Modern computational pathology frameworks typically rely on foundation models [1,3,14,15,23,24,29,32,34,36,41]. While differences exist between the various frameworks, they share the common idea to leverage representation models, able to map small patches of tissues (or tiles) to a lower

dimensional space by computing features (or embeddings). Those features can then later be aggregated to produce predictions or representations at slide level.

When designing CPath pipelines, two equally important questions arise: the model’s pure performance, and its robustness to variations in scanning conditions [16]. Recent studies have mostly focused on scaling the training dataset and the model size, resulting in large models whose size can reach more than one billion parameters, pretrained on several hundred thousands to a few million WSI [29,36,41]. This yielded spectacular improvements in performance on a variety of benchmarks and downstream tasks, yet, introduced an increased computational cost. Besides, the robustness of foundation models to variations in sample preparation (*e.g.*, staining) or digitization (*e.g.*, scanning) has not attracted the same attention as their performance despite being critical to the clinical deployment of CPath workflows. To further investigate this aspect, some datasets and benchmarks have been proposed, such as [9,22,25,35].

To jointly tackle the issue of the additional computational cost while promoting the robustness of the models, this study proposes to investigate the distillation of large foundation models. Starting from a recent foundation model, H-Optimus-0 [29], a Vision Transformer-giant (ViT-g) [10] with more than one billion parameters, we investigate its distillation into a smaller ViT-Base of 86 million parameters [10]. On several public benchmarks, the distilled model, H0-mini, demonstrates competitive performance with significantly larger state-of-the-art models. Additionally, leveraging the PLISM dataset [25], we show that the distilled model significantly outperforms all other foundation models reported in the literature for its robustness to variations in staining and scanning conditions. This uncovers new perspectives to design robust CPath models in view of their adoption in clinical practice. Our preprocessed version of PLISM dataset is publicly available for benchmark purposes at <https://huggingface.co/datasets/owkin/plism-dataset-tiles>.

## 2 Related work

### 2.1 Self-supervised learning (SSL) for digital pathology

Pretraining a feature extractor with SSL is now a cornerstone of modern CPath frameworks. First CPath pipelines used to leverage models pretrained on Imagenet [8], and suffered from an out-of-domain gap when transferred to digital pathology images. The advent of SSL methods showed the benefit of doing an in-domain pretraining for pathology feature extractors [5,7,27]. While it was originally leveraging contrastive methods [4,38] tailored for convolutional networks, more recent models build on the Vision Transformer (ViT) architecture, with pretraining methods coming such as DINO, iBOT or DINov2 [2,26,40]. Most of the recent foundation models for digital pathology leverage the DINov2 framework [23,29,35,36].

## 2.2 Distillation

Distillation is a well known machine learning technique that consists in supervising a student model by a teacher model [18]. In the context of building image foundation models, it has been shown to be more efficient to distill a large model into a smaller one rather than training the small model from scratch [26]. In [11], a simple method is proposed to perform the distillation, and variations corresponding to the various SSL frameworks are investigated. In particular, following the DINO and iBOT frameworks, two methods are proposed, namely RoB-DINO and RoB-iBOT. In the former, following the DINO self-distillation objective, the class token of the teacher serves to supervise the student. In the latter, following the iBOT masked image modeling objective, an additional loss term is added where the (unmasked) patch tokens of the teacher also serve to supervise the student.

While distillation techniques are well established in computer vision in general, their application to foundation models for digital pathology remains relatively scarce. In GPFM [23], 3 foundation models (CONCH, Phikon and UNI) are simultaneously distilled during the pre-training phase of the model in addition to the classical DINOv2 loss, aiming to capture “experts” knowledge in the resulting model. In [41], a ViT-Small model, Virchow2G-Mini is introduced. It results from the distillation of Virchow2G (a ViT-Giant) on a 1-billion tile dataset. The authors show that distillation is beneficial compared to pre-training the same ViT-Small model from scratch.

## 3 Material and methods

### 3.1 Pre-training setup

**Distillation setup** In this study, H-Optimus-0 is considered as the teacher model. We then follow the general methodology described in [26]. More precisely, for an image  $x$ , let  $x_1$  and  $x_2$  denote two augmented views of  $x$ . Additionally, for  $i \in \llbracket 1, 2 \rrbracket$ , we denote by  $z_i^{(t)}$  (resp.  $z_i^{(s)}$ ) the class tokens output by the teacher (resp. student) model for image  $x_i$ . For a patch  $p$ , we also denote by  $z_{i,p}^{(t)}$  (resp.  $z_{i,p}^{(s)}$ ) the patch tokens output by the teacher (resp. student) for the image  $x_i$ . We pass the teacher (resp. student) class tokens through the corresponding DINO head. This head is a MLP outputting a vector of scores, followed by softmax centering. Similarly, patch tokens are passed through either the teacher or student iBOT head. As a general notation,  $h_i$  corresponds to the head projection of  $z_i$ . Taking inspiration from [11], distillation is performed by combining two objectives:

- **DINO objective.** In this setting, only the class scores (derived from the projection of class tokens into the DINO heads) are used to perform the distillation. Let  $H$  denote the cross-entropy loss. The corresponding loss function  $L_{\text{dino}}$  is defined as

$$L_{\text{dino}} := \left( H(h_1^{(t)}, h_2^{(s)}) + H(h_2^{(t)}, h_1^{(s)}) \right) / 2.$$

- **iBOT objective.** The iBOT objective extends the distillation by incorporating patch tokens supervision. Only global crops are used to compute the objective. This loss is defined as the following

$$L_{\text{ibot}} := \frac{1}{2P} \sum_{p=1}^P \sum_{j=1}^2 H(h_{j,p}^{(t)}, h_{j,p}^{(s)}),$$

where  $P$  denotes the total number of patches. Unlike [11] we do not apply masking of the patches and the iBOT loss is applied for all patch scores (derived from the projection of patch tokens into the iBOT heads).

Finally, for all experiments, we keep a spare Exponential Moving Average (EMA) of the student as in [11] and we remove the stochastic depth. Separate heads for the DINO and iBOT distillation objectives are considered, and the Koleo regularizing loss is removed. To speed up the distillation, mixed precision is used as in [26]. We present in Table 4 the main parameters used for the distillation.

**Pre-training datasets** To assess the benefit of distillation compared to pre-training feature extractors from scratch, and similar to the Phikon setup [14], we perform the distillation on a dataset of 43M tiles extracted from 6,093 TCGA slides covering 16 cancer sites. Compared to the typical sizes of pre-training datasets, it stands out by its relatively small size. We note that this is a difference with the pretraining setup proposed in [41], where the distillation is performed on a 1B-tile dataset.

### 3.2 Evaluation setup

**Performance benchmarks** To rigorously evaluate model performance, we use two publicly available benchmarks<sup>1</sup>. The HEST-Benchmark [19] collects gene expression prediction tasks for 9 different indications. For each task, a subset of 50 highly variable genes is considered. To account for various embedding dimensions between feature extractors, we follow the recommended evaluation procedure from HEST-Benchmark, fitting a ridge regression on top of a PCA reduction with 256 components. We refer to the HEST paper and repository for more details on the evaluation procedure. Additionally, following the recommended methodology in [41], we use the concatenation of the class token and the mean over all patch tokens as embeddings of our distilled models. We note that because of the embedding dimension of ViT-Base models ( $d = 768$ ), concatenating the class token and the mean over all patch tokens results in embeddings of the same dimension as ViT-g models (*e.g.*, H0 or Gigapath) ( $d = 1536$ ).

We also leverage the EVA benchmark [17], which consists in 4 patch-level classification tasks, 2 patch-level segmentation tasks, and 2 slide-level classification tasks. For each category of tasks, EVA’s evaluation protocol is fixed to allow

---

<sup>1</sup> The HEST benchmark is available at <https://github.com/mahmoodlab/HEST>, and the EVA benchmark is available at <https://kaiko-ai.github.io/eva/main/>.

for a fair evaluation across feature extractors. For instance, the main hyperparameters such as learning rate, batch size, or schedulers are shared for all feature extractors. We refer to the EVA paper and documentation for more details on the evaluation procedure.

Our results can be reproduced on HEST-Benchmark and EVA’s respective code repositories.

**Robustness dataset** In order to evaluate model robustness, we use the public PLISM [25] dataset. PLISM consists of 46 human tissue types stained using 13 different H&E conditions, and captured using 7 WSI scanners. Of the 13 stainings, 3 were kept and 10 were discarded because they were deemed too different from routine H&E stainings. Each of those 21 experimental conditions consisted of one whole-slide image made of the 46 tissue punches. Those 21 WSIs were further aligned together using the Elastix software [21], taking the GMH-stained WSI captured with the Hamamatsu Nanozoomer S60 as reference. An in-house matter detection model was then used to detect tissue and tessellate those 21 WSIs into 16,278 tissue tiles each. Consequently, our robustness dataset is made of 16,278 tissue patches, each of them existing under 3 different H&E staining conditions and captured with 7 different scanners. We provide in Appendix 7.1 some visualizations from PLISM, following the registration step. Cosine similarity and top-k accuracy are used to evaluate the robustness of the feature extractors. These metrics are computed on slide pairs corresponding to different scanner and staining combinations.

- Cosine similarity is assessed on features extracted from tissue tiles, averaged over all 16,278 matching tile pairs. We note that this metric was proposed in [35] to quantify the robustness of feature extractors to stain normalization.
- Top-k accuracy computes the percentage of tiles from one slide whose matching tile on the other slide ranks among the k closest tiles (by cosine similarity) when compared to all other tiles from both slides. This metric is computed bidirectionally and averaged for each slide pair.

Finally, metrics are aggregated across unique combinations of distinct scanners and stainings, yielding a final robustness score for each feature extractor. We provide in Appendix 7.3 technical details on metrics computation. Specific robustness to scanner (resp. staining) is assessed on all intra-staining (resp. scanner) inter-scanner (resp. staining) pairs while overall robustness metrics is assessed using all pairs.

## 4 Results

### 4.1 HEST results

In Table 1, we report the results on the HEST benchmark. We notice that the distilled model performs remarkably well on this benchmark, highlighting the efficiency of knowledge distillation. The model significantly outperforms Phikon,

its equivalent trained from scratch (same architecture and same pre-training data). Additionally, both versions outperform in average much bigger foundation models such as Virchow2 or Prov-Gigapath.

**Table 1.** HEST results. Pearson correlations are reported for all tasks. For all models, [CLS] tokens are concatenated to the mean over all patch tokens to form the input embeddings.<sup>1</sup> For UNI 1.5, results are directly taken from HEST repository’s README.

Model	Size	IDC	PRAD	PAAD	SKCM	COAD	READ	ccRCC	LUAD	IDC	Average
H-Optimus-0	1,100M	<b>0.6106</b>	0.3621	<b>0.5106</b>	<b>0.6614</b>	0.3089	<b>0.2401</b>	<u>0.2669</u>	<u>0.5754</u>	<u>0.2664</u>	<b>0.4224</b>
UNI 1.5 <sup>1</sup>	-	<u>0.5989</u>	0.3645	0.4902	0.6401	0.2925	<u>0.2240</u>	0.2522	0.5586	<b>0.2695</b>	<u>0.4090</u>
<b>H0-mini</b>	86M	0.5909	0.3633	<u>0.5068</u>	0.6125	0.2700	0.2047	0.2643	0.5633	0.2640	0.4044
Virchow2	632M	0.5971	0.3528	0.4778	<u>0.6404</u>	0.2580	0.2073	0.2604	0.5685	0.2568	0.4019
Hibou Large	307M	0.5945	0.3231	0.4758	0.6059	<b>0.3128</b>	0.1823	<b>0.2777</b>	0.5720	0.2490	0.3992
Kaiko ViT-B/8	86M	0.5710	<u>0.3827</u>	0.4727	0.5904	<u>0.3105</u>	0.1726	0.2664	<b>0.5883</b>	0.2362	0.3912
UNI	307M	0.5851	0.3274	0.4882	0.6235	0.2583	0.1757	0.2463	0.5558	0.2576	0.3907
Prov-Gigapath	1,100M	0.5707	<b>0.3841</b>	0.4920	0.5823	0.3076	0.186	0.2277	0.5579	0.2499	0.3952
Phikon-V2	307M	0.5677	0.3793	0.4771	0.5845	0.2561	0.1865	0.2607	0.5502	0.2476	0.3897
Phikon	86M	0.5481	0.3452	0.4639	0.5555	0.2668	0.1667	0.2496	0.5679	0.2387	0.3780

## 4.2 EVA results

In Table 2, we report the results on the EVA benchmark. As suggested by the authors of the benchmark, we report the average results with and without the BACH task, as the spatial resolution of the images differ from the other tasks, and therefore tend to favor mixed-magnification models such as Virchow2 or the Kaiko models. Even though the results tend to saturate, with 6 models with an average performance (without BACH) between 0.78 and 0.79, similar conclusions from the HEST benchmark can be drawn. The distilled models are competitive with the other state-of-the-art models while being much smaller. A noticeable exception is the Kaiko-B/8 model which, with a similar architecture (but a smaller patch size which results in more computations), reaches equivalent performance. This shows that the distilled model can perform very well for a variety of tasks, including patch classification, WSI classification (ranking first) or segmentation.

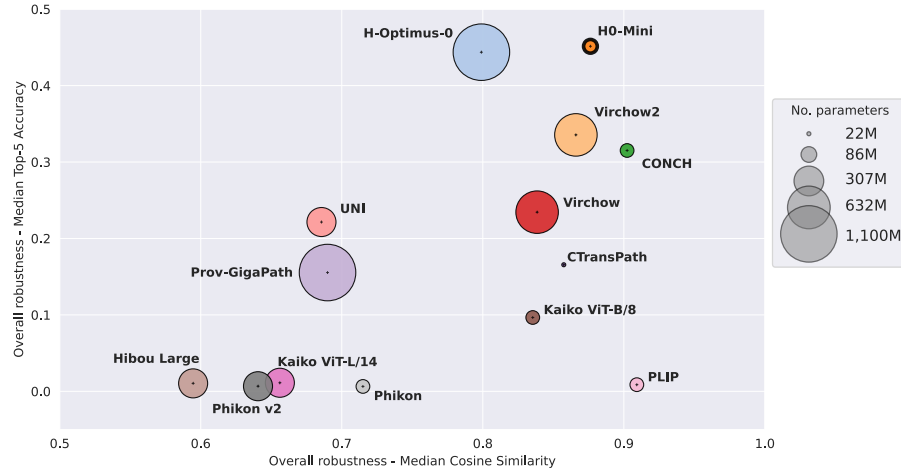
## 4.3 Robustness evaluation

Figure 1 presents the robustness metrics evaluated on the PLISM dataset. H0-mini achieves notably high scores, outperforming state-of-the-art models. We also note that multi-modal extractors, such as CONCH, demonstrate high robustness.

**Table 2.** EVA results. Balanced binary (resp. multiclass) accuracy is reported for binary (resp. multiclass) classification tasks. MonaiDiceScore is reported for segmentation tasks. For all models, input embeddings are only the [CLS] tokens. Following EVA benchmark, average performance is taken over all tasks except BACH.

Model	Size	Patch-level classification				Slide-level classification		Segmentation		Average
		BACH	CRC	MHIST	PCam	Cam16	PANDA	CoNSeP	MoNuSAC	
Virchow2	632M	<b>0.880</b>	<b>0.966</b>	<b>0.858</b>	0.936	<b>0.864</b>	0.642	0.630	0.663	<b>0.794</b>
H-Optimus-0	1,100M	0.758	<u>0.958</u>	0.839	0.942	0.820	0.645	0.637	<b>0.679</b>	<u>0.789</u>
Prov-Gigapath	1,100M	0.761	0.952	0.829	<u>0.945</u>	0.814	<u>0.664</u>	0.621	0.672	0.785
UNI	307M	0.797	0.947	<u>0.844</u>	0.936	0.834	0.656	0.628	0.638	0.783
<b>H0-mini</b>	86M	0.774	0.961	0.790	0.942	<u>0.842</u>	<b>0.667</b>	0.629	0.643	0.782
Hibou Large	307M	0.816	0.931	0.826	<b>0.951</b>	0.832	0.633	<u>0.642</u>	0.658	0.782
Kaiko ViT-B/8	86M	<u>0.858</u>	0.957	0.823	0.918	0.818	0.638	<b>0.645</b>	<u>0.675</u>	0.782
Phikon	86M	0.722	0.936	0.799	0.922	0.797	0.640	0.629	0.644	0.767
Phikon-V2	307M	0.727	0.939	0.775	0.893	0.808	0.635	0.630	0.639	0.760

We note that while there is a correlation between the cosine similarity metric and the retrieval metric, cosine similarity alone is not enough to assess the robustness of a foundation model. Models, such as PLIP and Phikon, present high values of cosine similarity, while failing at the retrieval task. Besides, robustness of a model should be evaluated alongside downstream performance, to have a comprehensive



**Fig. 1.** PLISM results - Median Top-5 Accuracy vs. Median Cosine Similarity by extractor. For both axes, higher values indicate more robust models.

understanding of a model’s behavior. It should also be noted that robustness to staining is harder to achieve compared to scanning as staining variations may have an impact on biological morphology (different stainings correspond to different consecutive cuts) while scanning variations mostly impact color tints. Figure 4 in Appendix 7.2 shows for all models their respective robustness with respect to scanning or staining variations based on Top-1 Accuracy. H0-Mini presents the highest robustness to scanning variations and ranks 3rd on staining robustness behind H-Optimus-0 and Virchow2.

## 5 Discussion

While the results presented in this work are very promising, several limitations and perspectives can be noted. First, we note that the final projection head of the teacher model is required to perform the distillation. Whether the distillation can be performed without the projection head (for instance, by learning them during the pre-training as in [23]) with equivalent downstream performance and robustness should be explored.

Second, even though distilled models will be much cheaper to use for downstream tasks (both in time, cost or energy consumption), it remains computationally demanding to obtain them compared to training a similar model from scratch (1.7x longer for a ViT-B architecture) as it requires the teacher model. However, the resulting performance and robustness is greatly improved.

Finally, we mention some open questions. The successful distillation of large models into smaller ones raises a question on the intrinsic dimension of foundation models in digital pathology, that should be further investigated. Besides, we did not perform an extensive hyperparameter optimization. Whether some could be tailored for distillation remains to be explored (*e.g.*, adding more global crops to the iBOT objective, reducing the student patch size, etc.). The choice of dataset on which to perform distillation may also have an impact on the downstream properties of the models.

## 6 Conclusion

This study shows that distilling a large foundation model results in a competitive smaller model. We show that this model can efficiently be leveraged for downstream applications closing the performance gap with larger foundation models. We hope our work will democratize the use of pathology foundation models for researchers with limited computational resources.

Besides, we show that distilled models present an additional robustness property, with their features having a better invariance to changes in scanners or staining conditions. Self-supervised learning is known to be an efficient way to address domain generalization in CPath [37] and, to the best of our knowledge, this study is the first to highlight that distilling a large foundation model further

improves the robustness of the resulting model. This enhanced robustness property lays the groundwork for future research, supporting the broader adoption of CPath models in clinical practice.

### 6.1 Acknowledgements.

*Computing resources.* This work was granted access to the High-Performance Computing (HPC) resources of IDRIS under the allocations 2023-A0141012519 and 2024-A0161012519 made by GENCI.

*Data access.* The results presented here are in part based upon data generated by the TCGA Research Network: <https://www.cancer.gov/tcga>.

## References

1. Alber, M., Tietz, S., Dippel, J., Milbich, T., Lesort, T., Korfiatis, P., Krügener, M., Cancer, B.P., Shah, N., Möllers, A., Seegerer, P., Carpen-Amarie, A., Standvoss, K., Dernbach, G., de Jong, E., Schallenberg, S., Kunft, A., von Ankershoffen, H.H., Schaeferle, G., Duffy, P., Redlon, M., Jurmeister, P., Horst, D., Ruff, L., Müller, K.R., Klauschen, F., Norgan, A.: Atlas: A novel pathology foundation model by mayo clinic, charité, and aignostics (2025). <https://doi.org/10.48550/ARXIV.2501.05409>, <https://arxiv.org/abs/2501.05409>
2. Caron, M.: Emerging properties in self-supervised vision transformers (Apr 2021), <https://arxiv.org/abs/2104.14294>
3. Chen, R.J., Ding, T., Lu, M.Y., Williamson, D.F.K., Jaume, G., Chen, B., Zhang, A., Shao, D., Song, A.H., Shaban, M., Williams, M., Vaidya, A., Sahai, S., Oldenburg, L., Weishaupt, L.L., Wang, J.J., Williams, W., Le, L.P., Gerber, G., Mahmood, F.: A general-purpose self-supervised model for computational pathology (arXiv:2308.15474) (Aug 2023). <https://doi.org/10.48550/arXiv.2308.15474>, <http://arxiv.org/abs/2308.15474>, arXiv:2308.15474 [cs, q-bio]
4. Chen, X., Fan, H., Girshick, R., He, K.: Improved baselines with momentum contrastive learning (arXiv:2003.04297) (Mar 2020). <https://doi.org/10.48550/arXiv.2003.04297>, <http://arxiv.org/abs/2003.04297>, arXiv:2003.04297 [cs]
5. Ciga, O., Xu, T., Martel, A.L.: Self supervised contrastive learning for digital histopathology. No. arXiv:2011.13971 (Sep 2021). <https://doi.org/10.48550/arXiv.2011.13971>, <http://arxiv.org/abs/2011.13971>, arXiv:2011.13971 [cs, eess]type: article
6. Courtiol, P., Maussion, C., Moarii, M., Pronier, E., Pilcer, S., Sefta, M., Manceron, P., Toldo, S., Zaslavskiy, M., Le Stang, N., Girard, N., Elemento, O., Nicholson, A.G., Blay, J.Y., Galateau-Sallé, F., Wainrib, G., Clozel, T.: Deep learning-based classification of mesothelioma improves prediction of patient outcome. *Nature Medicine* **25**(10), 1519–1525 (Oct 2019). <https://doi.org/10.1038/s41591-019-0583-3>
7. Dehaene, O., Camara, A., Moindrot, O., de Lavergne, A., Courtiol, P.: Self-Supervision Closes the Gap Between Weak and Strong Supervision in Histology. No. arXiv:2012.03583 (Dec 2020). <https://doi.org/10.48550/arXiv.2012.03583>, <http://arxiv.org/abs/2012.03583>, arXiv:2012.03583 [cs, eess]type: article

8. Deng, J., Dong, W., Socher, R., Li, L.J., Li, K., Fei-Fei, L.: Imagenet: A large-scale hierarchical image database. In: 2009 IEEE Conference on Computer Vision and Pattern Recognition. p. 248–255 (Jun 2009). [https://doi.org/10.1109/](https://doi.org/10.1109/CVPR.2009.5206848)  
[CVPR.2009.5206848](https://doi.org/10.1109/5206848)
9. Dippel, J., Feulner, B., Winterhoff, T., Milbich, T., Tietz, S., Schallenberg, S., Dernbach, G., Kunft, A., Heinke, S., Eich, M.L., Ribbat-Idel, J., Krupar, R., Anders, P., Preni&lsquo;fl, N., Jurmeister, P., Horst, D., Ruff, L., Müller, K.R., Klauschen, F., Alber, M.: Rudolfv: A foundation model by pathologists for pathologists (2024). <https://doi.org/10.48550/ARXIV.2401.04079>, <https://arxiv.org/abs/2401.04079>
10. Dosovitskiy, A., Beyer, L., Kolesnikov, A., Weissenborn, D., Zhai, X., Unterthiner, T., Dehghani, M., Minderer, M., Heigold, G., Gelly, S., Uszkoreit, J., Houlsby, N.: An image is worth 16x16 words: Transformers for image recognition at scale (arXiv:2010.11929) (Jun 2021), <http://arxiv.org/abs/2010.11929>, arXiv:2010.11929 [cs]
11. Duval, Q., Misra, I., Ballas, N.: A simple recipe for competitive low-compute self supervised vision models (2023). <https://doi.org/10.48550/ARXIV.2301.09451>, <https://arxiv.org/abs/2301.09451>
12. Ekholm, A., Wang, Y., Vallon-Christersson, J., Boissin, C., Rantanainen, M.: Prediction of gene expression-based breast cancer proliferation scores from histopathology whole slide images using deep learning. *BMC Cancer* **24**(1), 1510 (Dec 2024). <https://doi.org/10.1186/s12885-024-13248-9>
13. El Nahhas, O.S.M., Van Treeck, M., Wölflein, G., Unger, M., Ligero, M., Lenz, T., Wagner, S.J., Hewitt, K.J., Khader, F., Foersch, S., Truhn, D., Kather, J.N.: From whole-slide image to biomarker prediction: end-to-end weakly supervised deep learning in computational pathology. *Nature Protocols* **20**(1), 293–316 (Jan 2025). <https://doi.org/10.1038/s41596-024-01047-2>
14. Filiot, A., Ghermi, R., Olivier, A., Jacob, P., Fidon, L., Kain, A.M., Saillard, C., Schiratti, J.B.: Scaling self-supervised learning for histopathology with masked image modeling p. 2023.07.21.23292757 (Jul 2023). <https://doi.org/10.1101/2023.07.21.23292757>, <https://www.medrxiv.org/content/10.1101/2023.07.21.23292757v1>
15. Filiot, A., Jacob, P., Mac Kain, A., Saillard, C.: Phikon-v2, a large and public feature extractor for biomarker prediction (2024). <https://doi.org/10.48550/ARXIV.2409.09173>, <https://arxiv.org/abs/2409.09173>
16. Food, U., Administration, D.: Developing and labeling in vitro companion diagnostic devices for a specific group of oncology therapeutic products (Apr 2020), fDA-2018-D-3380
17. Gatopoulos, I., Käenzig, N., Moser, R., Otalora, S.: eva: Evaluation framework for pathology foundation models. *Medical Imaging with Deep Learning* (2024)
18. Hinton, G., Vinyals, O., Dean, J.: Distilling the knowledge in a neural network (2015). <https://doi.org/10.48550/ARXIV.1503.02531>, <https://arxiv.org/abs/1503.02531>
19. Jaume, G., Doucet, P., Song, A.H., Lu, M.Y., Almagro-Pérez, C., Wagner, S.J., Vaidya, A.J., Chen, R.J., Williamson, D.F.K., Kim, A., Mahmood, F.: Hest-1k: A dataset for spatial transcriptomics and histology image analysis (arXiv:2406.16192) (Jun 2024), <http://arxiv.org/abs/2406.16192>, arXiv:2406.16192 [cs]
20. Kather, J.N., Pearson, A.T., Halama, N., Jäger, D., Krause, J., Loosen, S.H., Marx, A., Boor, P., Tacke, F., Neumann, U.P., Grabsch, H.I., Yoshikawa, T., Brenner, H., Chang-Claude, J., Hoffmeister, M., Trautwein, C., Luedde, T.: Deep learning

can predict microsatellite instability directly from histology in gastrointestinal cancer. *Nature Medicine* **25**(77), 1054–1056 (Jul 2019). <https://doi.org/10.1038/s41591-019-0462-y>

21. Klein, S., Staring, M., Murphy, K., Viergever, M.A., Pluim, J.P.W.: elastix: a toolbox for intensity-based medical image registration. *IEEE Trans Med Imaging* **29**(1), 196–205 (Nov 2009)
22. Lee, J., Lim, J., Byeon, K., Kwak, J.T.: Benchmarking pathology foundation models: Adaptation strategies and scenarios (2024). <https://doi.org/10.48550/ARXIV.2410.16038>, <https://arxiv.org/abs/2410.16038>
23. Ma, J., Guo, Z., Zhou, F., Wang, Y., Xu, Y., Cai, Y., Zhu, Z., Jin, C., Lin, Y., Jiang, X., Han, A., Liang, L., Chan, R.C.K., Wang, J., Cheng, K.T., Chen, H.: Towards a generalizable pathology foundation model via unified knowledge distillation (2024). <https://doi.org/10.48550/ARXIV.2407.18449>, <https://arxiv.org/abs/2407.18449>
24. Nechaev, D., Pchelnikov, A., Ivanova, E.: Hibou: A family of foundational vision transformers for pathology (2024). <https://doi.org/10.48550/ARXIV.2406.05074>, <https://arxiv.org/abs/2406.05074>
25. Ochi, M., Komura, D., Onoyama, T., Shinbo, K., Endo, H., Odaka, H., Kakiuchi, M., Katoh, H., Ushiku, T., Ishikawa, S.: Registered multi-device/staining histology image dataset for domain-agnostic machine learning models. *Scientific Data* **11**(1), 330 (Apr 2024). <https://doi.org/10.1038/s41597-024-03122-5>
26. Oquab, M., Darcet, T., Moutakanni, T., Vo, H., Szafraniec, M., Khalidov, V., Fernandez, P., Haziza, D., Massa, F., El-Nouby, A., Assran, M., Ballas, N., Galuba, W., Howes, R., Huang, P.Y., Li, S.W., Misra, I., Rabbat, M., Sharma, V., Synnaeve, G., Xu, H., Jegou, H., Mairal, J., Labatut, P., Joulin, A., Bojanowski, P.: Dinov2: Learning robust visual features without supervision (arXiv:2304.07193) (Apr 2023). <https://doi.org/10.48550/arXiv.2304.07193>, <http://arxiv.org/abs/2304.07193>, arXiv:2304.07193 [cs]
27. Saillard, C.: Self supervised learning improves dmmr/msi detection from histology slides across multiple cancers (Sep 2021)
28. Saillard, C., Dubois, R., Tchita, O., Loiseau, N., Garcia, T., Adriansen, A., Carpentier, S., Reyre, J., Enea, D., Von Loga, K., Kamoun, A., Rossat, S., Wiscart, C., Sefta, M., Auffret, M., Guillou, L., Fouillet, A., Kather, J.N., Svrcek, M.: Validation of msintuit as an ai-based pre-screening tool for msi detection from colorectal cancer histology slides. *Nature Communications* **14**(1), 6695 (Nov 2023). <https://doi.org/10.1038/s41467-023-42453-6>
29. Saillard, C., Jenatton, R., Llinares-López, F., Mariet, Z., Cahané, D., Durand, E., Vert, J.P.: H-optimus-0 (2024), <https://github.com/bioptimus/releases/tree/main/models/h-optimus/v0>
30. Schmauch, B., Romagnoni, A., Pronier, E., Saillard, C., Maillé, P., Calderaro, J., Kamoun, A., Sefta, M., Toldo, S., Zaslavskiy, M., Clozel, T., Moarii, M., Courtiol, P., Wainrib, G.: A deep learning model to predict rna-seq expression of tumours from whole slide images. *Nature Communications* **11**(1), 3877 (Aug 2020). <https://doi.org/10.1038/s41467-020-17678-4>
31. Shao, Z., Bian, H., Chen, Y., Wang, Y., Zhang, J., Ji, X., Zhang, Y.: Transmil: Transformer based correlated multiple instance learning for whole slide image classification (Nov 2021), <https://openreview.net/forum?id=LKUfuWxajHc>
32. Vorontsov, E., Bozkurt, A., Casson, A., Shaikovski, G., Zelechowski, M., Liu, S., Mathieu, P., van Eck, A., Lee, D., Viret, J., Robert, E., Wang, Y.K., Kunz, J.D., Lee, M.C.H., Bernhard, J., Godrich, R.A., Oakley, G., Millar, E., Hanna,

M., Retamero, J., Moye, W.A., Yousfi, R., Kanan, C., Klimstra, D., Rothrock, B., Fuchs, T.J.: Virchow: A million-slide digital pathology foundation model (arXiv:2309.07778) (Sep 2023). <https://doi.org/10.48550/arXiv.2309.07778>, <http://arxiv.org/abs/2309.07778>, arXiv:2309.07778 [cs, eess, q-bio]

33. Wagner, S.J., Reisenbüchler, D., West, N.P., Niehues, J.M., Zhu, J., Foersch, S., Veldhuizen, G.P., Quirke, P., Grabsch, H.I., van den Brandt, P.A., Hutchins, G.G.A., Richman, S.D., Yuan, T., Langer, R., Jenniskens, J.C.A., Offermans, K., Mueller, W., Gray, R., Gruber, S.B., Greenson, J.K., Rennert, G., Bonner, J.D., Schmolze, D., Jonnagaddala, J., Hawkins, N.J., Ward, R.L., Morton, D., Seymour, M., Magill, L., Nowak, M., Hay, J., Koelzer, V.H., Church, D.N., consortium, T., Matek, C., Geppert, C., Peng, C., Zhi, C., Ouyang, X., James, J.A., Loughrey, M.B., Salto-Tellez, M., Brenner, H., Hoffmeister, M., Truhn, D., Schnabel, J.A., Boxberg, M., Peng, T., Kather, J.N.: Transformer-based biomarker prediction from colorectal cancer histology: A large-scale multicentric study. *Cancer Cell* **41**(9), 1650–1661.e4 (Sep 2023). <https://doi.org/10.1016/j.ccr.2023.08.002>

34. Wang, X.: Transformer-based unsupervised contrastive learning for histopathological image classification (Jul 2022)

35. Wölflein, G., Ferber, D., Meneghetti, A.R., Nahhas, O.S.M.E., Truhn, D., Carrero, Z.I., Harrison, D.J., Arandjelović, O., Kather, J.N.: Benchmarking pathology feature extractors for whole slide image classification (2023). <https://doi.org/10.48550/ARXIV.2311.11772>, <http://arxiv.org/abs/2311.11772>

36. Xu, H., Usuyama, N., Bagga, J., Zhang, S., Rao, R., Naumann, T., Wong, C., Gero, Z., González, J., Gu, Y., Xu, Y., Wei, M., Wang, W., Ma, S., Wei, F., Yang, J., Li, C., Gao, J., Rosemon, J., Bower, T., Lee, S., Weerasinghe, R., Wright, B.J., Robicsek, A., Piening, B., Bifulco, C., Wang, S., Poon, H.: A whole-slide foundation model for digital pathology from real-world data. *Nature* **630**(8015), 181–188 (Jun 2024). <https://doi.org/10.1038/s41586-024-07441-w>

37. Zamanitajeddin, N., Jahanifar, M., Xu, K., Siraj, F., Rajpoot, N.: Benchmarking domain generalization algorithms in computational pathology (arXiv:2409.17063) (Sep 2024), <http://arxiv.org/abs/2409.17063>, arXiv:2409.17063 [cs]

38. Zbontar, J., Jing, L., Misra, I., LeCun, Y., Deny, S.: Barlow Twins: Self-Supervised Learning via Redundancy Reduction. No. arXiv:2103.03230 (Jun 2021). <https://doi.org/10.48550/arXiv.2103.03230>, <http://arxiv.org/abs/2103.03230>, arXiv:2103.03230 [cs, q-bio] type: article

39. Zhang, H., Meng, Y., Zhao, Y., Qiao, Y., Yang, X., Coupland, S.E., Zheng, Y.: Dtdfd-mil: Double-tier feature distillation multiple instance learning for histopathology whole slide image classification. 2022 IEEE/CVF Conference on Computer Vision and Pattern Recognition (CVPR) p. 18780–18790 (Jun 2022). <https://doi.org/10.1109/CVPR52688.2022.01824>

40. Zhou, J., Wei, C., Wang, H., Shen, W., Xie, C., Yuille, A., Kong, T.: ibot: Image bert pre-training with online tokenizer (arXiv:2111.07832) (Jan 2022). <https://doi.org/10.48550/arXiv.2111.07832>, <http://arxiv.org/abs/2111.07832>, arXiv:2111.07832 [cs]

41. Zimmermann, E., Vorontsov, E., Viret, J., Casson, A., Zelechowski, M., Shaikovski, G., Tenenholz, N., Hall, J., Klimstra, D., Yousfi, R., Fuchs, T., Fusi, N., Liu, S., Severson, K.: Virchow2: Scaling self-supervised mixed magnification models in pathology (2024). <https://doi.org/10.48550/ARXIV.2408.00738>, <http://arxiv.org/abs/2408.00738>

## 7 Supplemental

### 7.1 PLISM dataset visualization

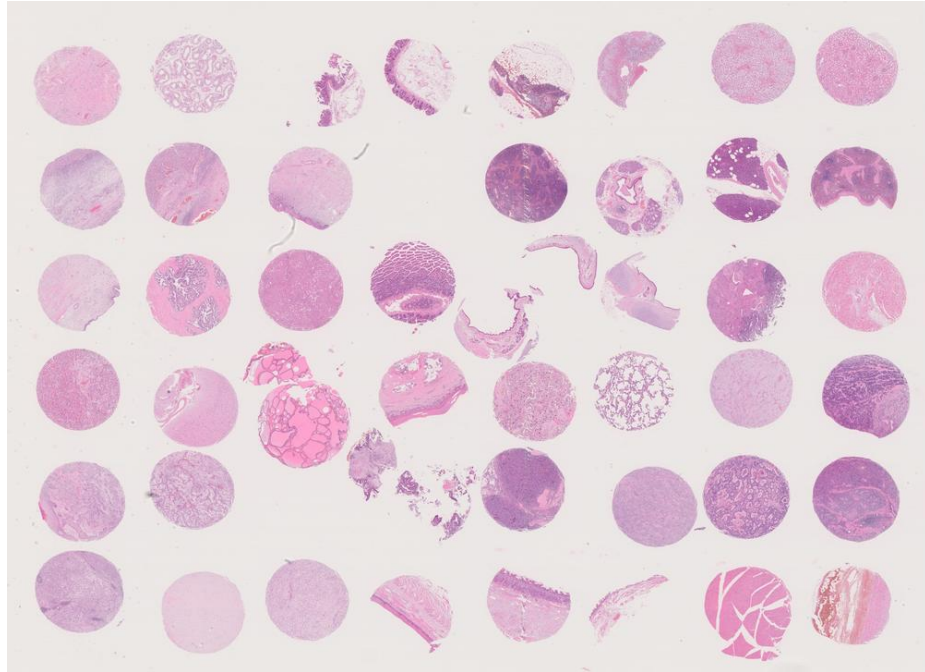


**Fig. 2.** Thumbnail of PLISM dataset slide serving as reference for registration. This WSI is stained with GMH condition and digitized using Hamamatsu Nanozoomer S60 scanner.

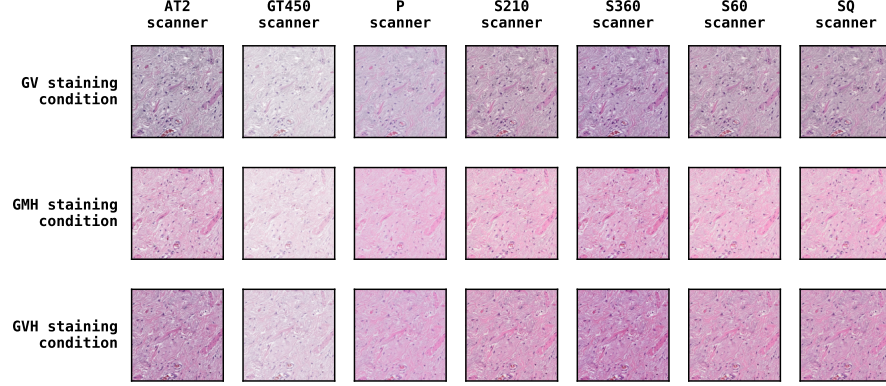


**Fig. 3.** Detailed view of one tile in the PLISM dataset after registration. Horizontally, the variability introduced by varying the scanner can be visualized, and vertically, the variability introduced by the staining conditions.

## 7.2 Additional PLISM dataset results

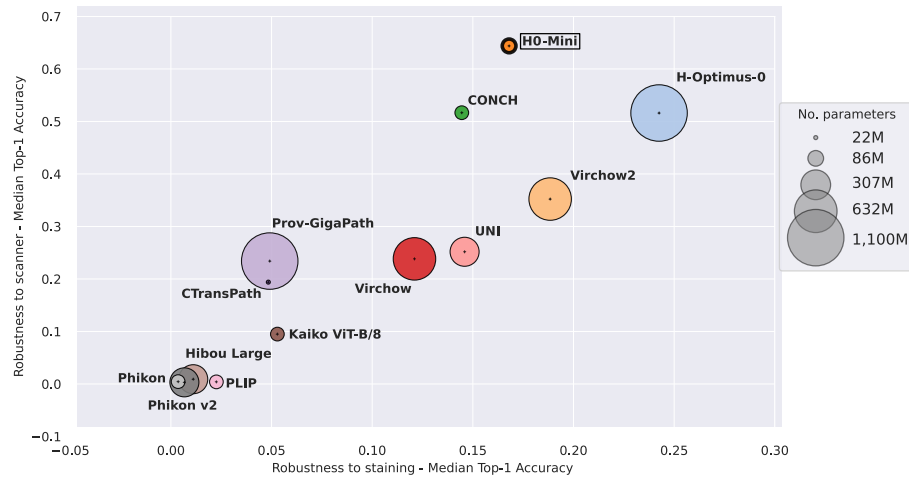


**Fig. 4.** PLISM results - Robustness to scanner vs robustness to staining as measured by median Top-1 Accuracy.

**Table 3.** PLISM results - Detailed metrics for all extractors. For each metric, median (inter-quartile range) is reported.

Model	Cosine Similarity	Top-1 Accuracy	Top-5 Accuracy
H0-Mini	0.876 (0.075)	0.239 (0.430)	<b>0.451 (0.501)</b>
H-Optimus-0	0.799 (0.108)	<b>0.261 (0.375)</b>	0.444 (0.431)
Virchow 2	0.866 (0.070)	0.162 (0.244)	0.336 (0.325)
CONCH	0.902 (0.065)	0.154 (0.389)	0.315 (0.507)
Virchow	0.838 (0.088)	0.110 (0.202)	0.234 (0.265)
UNI	0.686 (0.172)	0.081 (0.219)	0.222 (0.357)
CTransPath	0.857 (0.090)	0.056 (0.173)	0.166 (0.324)
Prov-Gigapath	0.690 (0.169)	0.054 (0.201)	0.155 (0.345)
Kaiko ViT-B/8	0.835 (0.088)	0.024 (0.100)	0.097 (0.227)
Hibou Large	0.595 (0.149)	0.002 (0.011)	0.010 (0.034)
PLIP	<b>0.909 (0.047)</b>	0.001 (0.016)	0.009 (0.055)
Phikon-V2	0.641 (0.16)	0.001 (0.006)	0.007 (0.027)
Phikon	0.715 (0.178)	0.001 (0.005)	0.006 (0.028)

### 7.3 Mathematical details of robustness evaluation metrics

**Cosine Similarity between Tiles** The cosine similarity between two tiles is a measure of the similarity between their feature vectors. Let  $t_1$  and  $t_2$  represent the feature vectors of two tiles. The cosine similarity between  $t_1$  and  $t_2$  is defined as:

$$\text{Cosine Similarity}(t_1, t_2) = \frac{\langle t_1, t_2 \rangle}{\|t_1\|_2 \|t_2\|_2},$$

where

- $\langle \cdot, \cdot \rangle$  denotes the canonical dot product,
- and  $\|\cdot\|_2$  denotes the corresponding euclidean norm.

**Cosine Similarity for a Slide Pair** For each slide pair  $(S_1, S_2)$ , the Mean Cosine Similarity is computed by averaging the cosine similarities between corresponding tile pairs. Each tile pair  $(t_{i,1}, t_{i,2})$  corresponds to a matched location, where  $t_{i,1}$  and  $t_{i,2}$  are the feature vectors extracted from slides  $S_1$  and  $S_2$ , respectively. Let  $N$  denote the total number of tile pairs. The Mean Cosine Similarity between  $S_1$  and  $S_2$  is then:

$$\text{Mean Cosine Similarity}_{S_1, S_2} = \frac{1}{N} \sum_{i=1}^N \text{Cosine Similarity}(t_{i,1}, t_{i,2}).$$

**Top-k Accuracy for a Slide Pair** For each tile  $t_{i,1}$  from slide  $S_1$ , the cosine similarities between  $t_{i,1}$  and all other tiles from both  $S_1$  and  $S_2$  are computed. These tiles are then ranked based on their similarity. The Top-k Accuracy is defined as the fraction of tiles from  $S_1$  whose corresponding tile from  $S_2$  ranks among the top  $k$  closest tiles. Formally, the Top-k Accuracy from  $S_1$  to  $S_2$  is:

$$\text{Top-k Accuracy}_{S_1 \rightarrow S_2} = \frac{1}{N} \sum_{i=1}^N \mathbb{1}(\text{rank}_{S_1 \cup S_2}(t_{i,2}) \leq k),$$

where the rank of  $t_{i,2}$  in  $S_1 \cup S_2$  is defined as:

$$\text{rank}_{S_1 \cup S_2}(t_{i,2}) = |\{t \in (S_1 \cup S_2), t \neq t_{i,1} : \text{Cosine Similarity}(t_{i,1}, t) \geq \text{Cosine Similarity}(t_{i,1}, t_{i,2})\}|.$$

The final Top-k Accuracy for the slide pair is obtained by averaging the Top-k Accuracy in both directions:

$$\text{Top-k Accuracy}_{S_1, S_2} = \frac{1}{2} (\text{Top-k Accuracy}_{S_1 \rightarrow S_2} + \text{Top-k Accuracy}_{S_2 \rightarrow S_1}).$$

#### 7.4 Distillation hyperparameters

Finally, we provide in Table 4 the main hyperparameters used in the distillation.

**Table 4.** Main hyperparameters used in the distillation.

---

<b>Optimization</b>	Warmup epochs	16
<b>Parameters</b>	Teacher temperature warmup epochs	30
	Weight decay end value	0.4
	Total batch size	2,048
	Number of iterations	105,000
<b>Model</b>	Patch size	14
<b>Parameters</b>	Register tokens	4
	Embedding dimension	768
	Layers	12
	Heads	12
	MLP ratio	4
	MLP activation	SwiGLU
<b>Projection</b>	Heads prototypes	131,072
<b>Heads</b>	DINO head bottleneck dim	384
	iBOT head bottleneck dim	256
<b>Hardware</b>	GPUs	128 V100 32 Go

---